Biophysical Journal Volume 80 February 2001 801–811

Structure, Location, and Lipid Perturbations of Melittin at the Membrane Interface

Kalina Hristova,* Christopher E. Dempsey,† and Stephen H. White*

*Department of Physiology and Biophysics and the Program in Macromolecular Structure, University of California at Irvine, Irvine, California 92697-4560 USA and †Department of Biochemistry, School of Medical Sciences, University of Bristol, Bristol, BS8 1TD, United Kingdom

ABSTRACT Melittin is arguably the most widely studied amphipathic, membrane-lytic α-helical peptide. Although several lines of evidence suggest an interfacial membrane location at low concentrations, melittin's exact position and depth of penetration into the hydrocarbon core are unknown. Furthermore, the structural basis for its lytic action remains largely a matter of conjecture. Using a novel x-ray absolute-scale refinement method, we have now determined the location, orientation, and likely conformation of monomeric melittin in oriented phosphocholine lipid multilayers. Its helical axis is aligned parallel to the bilayer plane at the depth of the glycerol groups, but its average conformation differs from the crystallographic structure. As observed earlier for another amphipathic α-helical peptide, the lipid perturbations induced by melittin are remarkably modest. Small bilayer perturbations thus appear to be a general feature of amphipathic helices at low concentrations. In contrast, a dimeric form of melittin causes larger structural perturbations under otherwise identical conditions. These results provide direct structural evidence that self-association of amphipathic helices may be the crucial initial step toward membrane lysis.

INTRODUCTION

Detailed structural and thermodynamic information about amphipathic α-helical peptides in membranes is important because of the widespread occurrence of the motif in host-defense peptides and membrane proteins. The most extensively studied of such peptides is undoubtedly melittin (MLT) (Habermann, 1972), the 26-residue membrane-lytic (Sessa et al., 1969) peptide isolated from the venom of the European honeybee *Apis mellifera* (reviewed in Dempsey, 1990). Nevertheless, little structural information about MLT in membranes is available beyond the basic facts that it forms, at low membrane concentrations, monomeric (Altenbach and Hubbell, 1988; John and Jähnig, 1991) α-helices in the membrane interface arranged parallel to the bilayer plane (Frey and Tamm, 1991; John and Jähnig, 1991; Dempsey and Butler, 1992; Okada et al., 1994; White et al., 1998; Ladokhin and White, 1999). The exact location, however, of MLT in the interface has remained a matter of speculation. The lack of a precise location is evident in recent molecular dynamics simulations in which the starting configurations place MLT in positions ranging from outside the headgroup region (Lin and Baumgärtner, 2000) to positions deep within the interface, with a variety of orientations (Bernèche et al., 1998; Bachar and Becker, 1999, 2000). We present here x-ray diffraction results that precisely pinpoint the location and orientation of MLT in a membrane interface.

At higher concentrations, MLT permeabilizes membranes by forming ~25-Å diameter pores (Katsu et al., 1988; Ladokhin et al., 1997a) thought to consist (Vogel and Jähnig, 1986) of transmembrane helices in a barrel-stave arrangement (Baumann and Mueller, 1974; Fox and Richards, 1982; Hall et al., 1984), possibly containing interspersed lipids (Matsuzaki et al., 1997). The helical structure of MLT in fluid membranes is frequently assumed to be identical (Bernèche et al., 1998) with the crystallographic structure (Terwilliger and Eisenberg, 1982a,b), although nuclear magnetic resonance (NMR) studies suggest otherwise (Dempsey and Butler, 1992; Okada et al., 1994). The structure of the MLT monomer in tetrameric crystals, grown from high ionic strength aqueous solutions (Terwilliger and Eisenberg, 1982a,b), consists of two α-helical segments separated by a characteristic kink at Pro^{14}. For MLT in membranes, Terwilliger et al. (1982) conjectured that the crystal structure is largely preserved and arranged with the plane of the kink perpendicular to the membrane. Although this structure is suggestive and forms the basis for barrel-stave pore models (Vogel and Jähnig, 1986), MLT-induced membrane permeabilization is only vaguely understood. Kinetic studies suggest helix association on the membrane as a precursor of pore formation, with dimerization being the rate-limiting step in many (DeGrado et al., 1982; Schwarz and Beschiaschvili, 1989; Schwarz et al., 1992), but not all (Rex and Schwarz, 1998), cases. Recently, Takei et al. (1999) provided direct evidence for the kinetic importance of MLT association in pore formation through studies of cysteine-substituted MLT pairs linked by disulfide bridges. We examine here one such pair formed from a substitution of Cys for Gln at position 25.

Received for publication 14 July 2000 and in final form 17 November 2000.

Abbreviations used: MLT, melittin: GIGAVLKVLTTLPALISWIKRKRQ^{25}Q-amide; AC-18A-NH_2, acetyl-DWLKAFYDKVAEKLKEAF-amide; Q25C, a disulfide-linked dimer of MLT Cys-substituted at position 25 (GIGAVLKVLTTLPALISWIKRKRC^{25}Q-amide).

Address reprint requests to Stephen H. White, Department of Physiology and Biophysics, Med. Sci. I, D346, University of California at Irvine, Irvine, CA 92697-4560. Tel.: 949-824-7122; Fax: 949-824-8540; E-mail: shwhite@uci.edu.

0006-3495/01/02/801/11 $2.00

We consider four questions: Does the conformation of MLT in fluid bilayers differ from what is observed in the crystal structure, as suggested by NMR studies? What is the location and orientation of MLT in bilayers? To what extent is the bilayer perturbed by MLT monomers? Does dimerization increase the perturbations? We have sought answers to these questions using a novel absolute-scale x-ray diffraction method previously applied to another amphipathic helical peptide, Ac-18A-NH_2 (Hristova et al., 1999). Specifically, we have examined MLT and a cysteine-linked dimeric MLT (Q25C) in oriented multilamellar bilayer arrays formed from dioleoylphosphatidylcholine (DOPC) at 66% relative humidity (RH). The results show, as for Ac-18A-NH_2, that monomeric MLT causes only minor changes in bilayer structure. This suggests that a general feature of amphipathic helices in membrane interfaces at low concentrations is small bilayer perturbations. In contrast, several small peptides and Q25C cause significantly larger perturbations.

MATERIALS AND METHODS

Materials

DOPC and 1-oleoyl-2-(9,10-dibromostearoyl)-*sn*-glycero-3-phosphocholine (OBPC) were purchased from Avanti Polar Lipids (Alabaster, AL). Purity of OBPC was determined by elemental analysis to be >99.9% (Microlit Laboratories, Madison, NJ). MLT, HPLC purified, was purchased from Sigma (St. Louis, MO). This grade of MLT, though not listed in the Sigma catalog, can be ordered using catalog number M1407. Q25C was synthesized and characterized as described elsewhere (Takei et al., 1999).

Membrane composition and oriented circular dichroism

Water contents of oriented multilayers with peptides were determined gravimetrically as described previously (Hristova et al., 1999). The nature and number of counterions in peptide samples were determined after lyophilizing solutions of the peptide and pumping under high vacuum, followed by solution NMR in D_2O to identify and quantitate counterions by integration. Oriented circular dichoroism (OCD) was carried out on samples prepared in exactly the same manner as those used for diffraction studies, as described previously (Hristova et al., 1999), following the approach of Huang and colleagues (Wu et al., 1990).

X-ray diffraction

Lipid and MLT (1 mol%) were codissolved in methanol, and then deposited on a curved glass substrates in the manner previously described (Wiener and White, 1991c; Hristova and White, 1998). RH was maintained at 66% with a saturated solution of $NaNO_2$. The sample was placed in a custom-made humidity chamber with thin x-ray-transparent beryllium windows. The curved surface of the substrate was placed in the x-ray beam in a manner that permitted all lamellar diffraction orders to be recorded in a single experiment. In this geometry, most of the wide-angle scattering, due, for example, to the lipid acyl chains, was absorbed by the glass substrate (Wiener and White, 1991c). Because of the thermal motion of the bilayer and the presence of the peptide, only five orders of diffraction data were observable, compared to the eight orders observed in the absence of MLT. The peptide, in essence, smoothes out the more rugged peptide-free bilayer profile. Five orders of diffraction thus yield fully resolved peptide–bilayer profiles, as discussed below and more extensively elsewhere (Hristova et al., 1999).

"Fully resolved" means that five orders of diffraction ($h = h_{max}$) is the maximum number observable. That is, the shape of the profile is such that no more than five orders can be produced by diffraction, even though the lattice is nearly perfect. The confusing issue of resolution in lamellar diffraction has been discussed in detail by Wiener and White (1991a). Particularly confusing is the meaning of the canonical resolution, defined as d/h_{max} where d is the Bragg spacing (unit cell dimension). With $d \sim 50$ Å, the canonical resolution is ~10 Å in these experiments. This number is a measure of the thermal disorder of the system in the absence of lattice disorder, as in our experiments. In other words, the scattering atoms are spread out over a significant fraction of the unit cell, on the time scale of the diffraction experiment. The result is a broad, smooth electron density envelope that requires no more than h_{max} terms for a faithful Fourier reconstruction from the diffracted intensities. This canonical resolution is often confused with what White and Wiener (1995, 1996) have dubbed "resolution precision," which is the precision of determining the position and width of the smooth envelope of electron density within the unit cell. The resolution precision depends upon the relative scattering strength of the envelope and its position in the unit cell, but is typically smaller than 0.5 Å (Wiener and White, 1991a), and can be as small as 0.01 Å. Consequently, we were able to determine the positions and widths of the MLT envelope and Br-labeled double-bonds with excellent precision.

Sample degradation was monitored by thin layer chromatography (TLC) and high performance liquid chromatography (HPLC). For typical exposure times of 8–10 h, no degradation was detected. Furthermore, no systematic differences in the line widths or integrated intensities were observed. X-ray diffraction measurements were performed with CuK_α radiation using a rotating anode x-ray generator (Bruker AXS (formerly Siemens), Madison, WI) operated at 38 kV and 30 mA. Double-focusing optics (Charles Supper, Nattick, MA) were used to focus the beam at the detector. The diffraction pattern was recorded on a Siemens X-1000 xenon-filled area detector with position-decoding circuit and real-time data display. The collection of x-ray data, peak integration, and absorption corrections were performed as described extensively elsewhere (Hristova and White, 1998). Experimental uncertainties for each peak were obtained from the statistical uncertainties of the integrated intensities of the diffraction peaks taken as $(\text{peak area} + \text{background})^{1/2}$. As discussed below, complete x-ray data sets were collected using six different OBPC:DOPC mole fractions ranging from 0 to 0.50. This procedure, used for both MLT and Q25C, is equivalent to six experimental determinations of structure factors and Bragg spacing.

Absolute-scale structure refinement

Lamellar diffraction is the only method available for the direct determination of the structure of lipid membranes in their natural fluid state (Franks and Levine, 1981). Fourier inversion of the diffracted intensities of x-rays or neutrons obtained from multilamellar arrays of fluid bilayers yields one-dimensional scattering-length density "profiles" (e.g., Fig. 1) that represent the projection of the highly thermally disordered contents of the unit cell onto the bilayer normal (Wiener and White, 1991a). The profiles are usually determined on a relative scale, i.e., the amplitudes of the electron density fluctuations around the mean density are displayed on an arbitrary scale. Although these relative-scale profiles provide useful rudimentary information about bilayer structure, we have demonstrated (Hristova et al., 1999) that they provide little or no insight into the disposition of peptides within bilayers. The usefulness of lamellar diffraction experiments is improved dramatically by determining profiles on an absolute scale, as first shown by MacNaughtan et al. (1985). Importantly, absolute scaling ties profiles directly to the composition and physical density of the bilayer (Franks et al., 1978; Wiener and White, 1991a; Hristova and White,

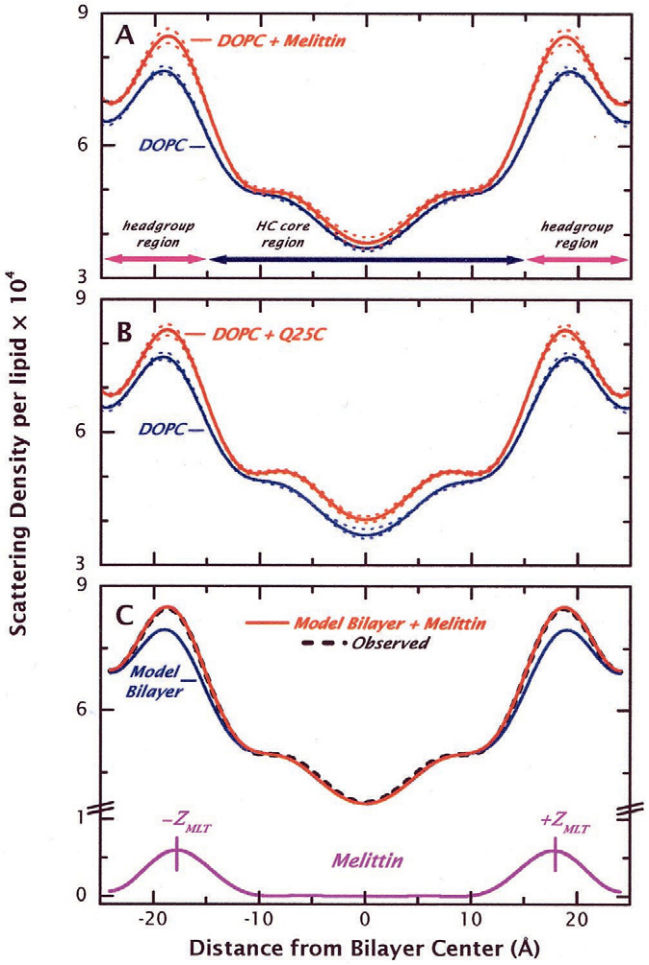

FIGURE 1 Scattering-length density profiles on the absolute per-lipid scale for DOPC multilayers with (*red curves*) and without (*blue curves*) MLT or Q25C, and for MLT alone (*violet curve*, panel *C*). The approximate extents of the headgroup and HC core regions of the bilayer are indicated schematically by the pink and dark blue arrows at the bottom of panel *A*. The origin of the scaling factor 10^4 is described in Appendix. (*A*) Profiles associated with monomeric MLT. The location of MLT in the headgroup region of the bilayer is apparent from a comparison of DOPC + MLT profile with the DOPC profile. Notice the very small difference between the curves in the HC core region, which is indicative of minor perturbations in that region. OCD measurements show the MLT is highly helical and oriented parallel to the bilayer plane (Fig. 4). (*B*) Profiles associated with dimeric MLT (Q25C). The difference in density between the DOPC + Q25C and the DOPC curves still shows considerable density in the headgroup region. Notice, however, the very significant difference in density in the HC core region. The structural perturbations induced by Q25C are so severe as to prevent direct determination of the location of Q25C by the absolute-scale refinement method. OCD measurements, however, show that Q25C is highly helical and oriented parallel to the membrane plane (Fig. 4). (*C*) Profiles summarizing the results of the absolute-scale refinement of the structure of DOPC bilayers containing 1 mol% MLT (see text). The experimentally observed profile is shown by the black dashed curve. The model structure, shown by the red curve, results from Fourier synthesis from the summed structure factors for the model of the perturbed bilayer (*blue curve*) and the refined MLT distribution (*violet curve*).

1998; Hristova et al., 1999). Although absolute-scale profiles are often presented in units of electrons per unit volume (electron density), we generally use scattering-length density units because they are more appropriate when x-ray data and neutron data are combined in so-called composition space refinement (Wiener and White, 1991b). As discussed in the Appendix, scattering-length density is obtained by multiplying electron density by mc^2/e^2. The most convenient scattering-length absolute scale is the so-called per-lipid scale (Hristova et al., 1999), which has the advantage of not requiring direct knowledge of the area per lipid (see the Appendix). Regardless of the units used, it is the differences in densities between profiles in the presence and absence of peptide that matter. The computation of the positions and widths of Gaussian profile features is unaffected by the choice of units.

Wiener and White (1991a,b) showed that combined x-ray and neutron experiments using heavy-atom specific labeling not only allow profiles to be placed on an absolute scale, but permit their decomposition into a collection of Gaussian component distributions as well. Each distribution represents the time-averaged projection of the motions of the water and principal lipid structural (component) groups (carbonyls, double-bonds, phosphate, etc.) onto the bilayer normal. The distributions taken as a group account for the contents of the unit cell and comprise the structure of a fluid bilayer (e.g., Fig. 2 *A*). The positions and widths of the Gaussians are obtained by joint refinement of x-ray and neutron data using a crystallographic approach, referred to as liquid-crystallography (see reviews in White and Wiener, 1995, 1996). The absolute-scale x-ray refinement method (Hristova et al., 1999) we employ here uses, as a starting point, the complete liquid-crystallographic structure of a peptide-free fluid bilayer, in this case DOPC at 66% RH (Wiener and White, 1992).

In the presence of a peptide, the structure of the peptide–bilayer complex is given by the superposition of the transbilayer distribution of the peptide with the set of component distributions of the peptide-perturbed lipid bilayer. The object of absolute-scale refinement is to determine these distributions. As described in detail elsewhere (Hristova et al., 1999), refinement involves four steps: 1) Determination of the x-ray scattering-length density profiles of the bilayer with and without peptide on the per-lipid absolute scale. This is accomplished by means of an isomorphous marker-lipid (OBPC) equivalent to DOPC brominated at the 9,10-double-bond of the *sn*-2 chain through an addition reaction (Wiener and White, 1991c). This step also yields the transbilayer double-bond distribution in the presence and absence of peptide, as shown by Wiener and White (1991c). Importantly, this distribution serves as a general measure of the state of the bilayer hydrocarbon (HC) core (Hristova and White, 1998). 2) Construction of peptide-perturbed bilayer model structures derived from changes in Bragg spacing and the double-bond distribution. This step is essential because the peptide causes the bilayer structure and the contents and dimensions of the unit cell to change. 3) Determination of the best transbilayer Gaussian distribution for the peptide. We have shown by molecular dynamics simulations that a Gaussian distribution accurately describes the transbilayer distribution of peptides in highly thermally disordered bilayers (Hristova et al., 1999). 4) Determination, by model building, of the range of peptide conformations, positions, and orientations that best satisfy this distribution. The successful application of our approach depends, however, on the peptide-induced bilayer structural changes being small enough to allow the perturbed bilayer to be modeled from the unperturbed bilayer in Step 2 by a simple scaling procedure (below) (Hristova et al., 1999). We found that the method could be applied successfully for monomeric MLT, but not dimeric Q25C. This means that the perturbations caused by the dimeric form are substantial.

Refinement procedures

Absolute-scale bilayer profiles

All bilayer profiles were placed on the absolute per-lipid scale using mixtures of DOPC and an isomorphous variant (OBPC) brominated at the

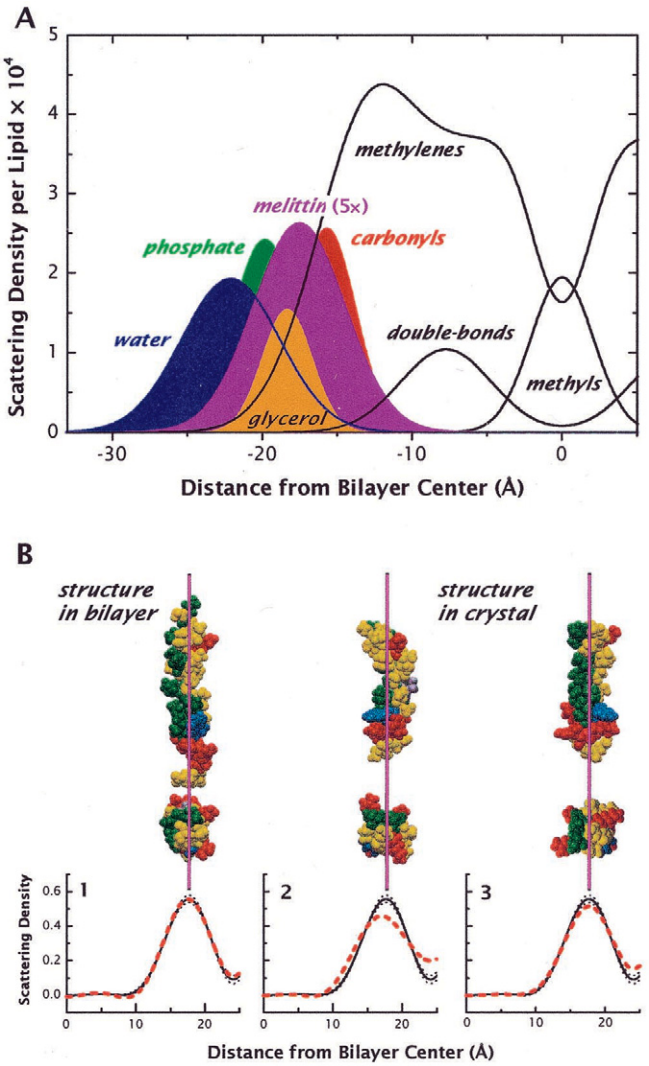

FIGURE 2 Disposition of MLT in oriented DOPC bilayers. (*A*) The transbilayer distribution of MLT (*violet*) in the context of the component distributions of the peptide-perturbed model bilayer. The structure of the bilayer is given by the complete set of Gaussian component distributions that account for the contents of the unit cell (see text). For clarity, the distribution of the choline group is not shown and the amplitude of the MLT distribution has been multiplied by 5. These distributions were obtained from the structure of the neat DOPC bilayer (see legend, Fig. 1). The thermally disordered surface of the helix penetrates the bilayer to the level of the double bonds. The acetyl counterions that accompany MLT into the bilayer are included with the water distribution in this model. The MLT helix axis is located at $Z_{MLT} = 17.5\ (\pm 0.2)$ Å from the bilayer center, close to the glycerol moiety (*orange*), and has a 1/*e*-halfwidth $A_{MLT} = 4.3\ (\pm 0.4)$ Å. Although the exact location of the acetyl counterions at low hydration is uncertain, other placements have little effect on the results. If they are included with the MLT distribution, then $Z_{MLT} = 17.9\ (\pm 0.2)$ Å and $A_{MLT} = 4.6\ (\pm 0.4)$ Å. If the counterions are neglected altogether, then $Z_{MLT} = 17.9\ (\pm 0.2)$ Å and $A_{MLT} = 4.4\ (\pm 0.4)$ Å. (*B*) Scattering-length density profiles of MLT models (*red dotted lines*) compared to the experimentally determined MLT profile (*black curves*; dotted lines indicate experimental uncertainty). The orientation of the bilayer plane for the models is perpendicular to the plane of the page, as shown by the pink bars. The amino acids in the molecular models are color coded according to the interfacial hydrophobicity scale of Wimley and White (1996): Tryptophan, blue; leucine and isoleucine, green; alanine, valine, threonine, glycine, yellow; lysine and arginine, red. Pro^{14} is colored gray for easier identification. The optimum average *B*-factor for a particular structural model was obtained from the best fit of the model's profile to the observed MLT profile (Fig. 1 *C*) using the refinement procedure described in Materials and Methods. If the calculated *B*-factors were of the order of the *B*-factor for the glycerol moiety (Hristova et al., 1999) (78 Å^2) or higher (but <200 Å^2), the conformation was considered consistent with the data. Because the thermal motion of the peptide is tightly coupled to the thermal motion of the bilayer, the peptide *B*-factors should fall within this range. The *B*-factor for the model in panel 1 was found to be 140 Å^2. For panels 2 and 3, the optimal *B*-factors for the crystal structures are ~ 0 Å^2, which rules them out as realistic models. For purposes of comparison, however, we have applied nominal *B*-factors of 140 Å^2 for the crystal structures used in panels 2 and 3. (*1*) The fit of a helical model that is generally consistent with NMR (Dempsey and Butler, 1992; Okada et al., 1994) and EPR (Altenbach et al., 1989) data. The first 22 residues in this model form an α-helix and the last 4 charged residues are extended along the helix axis. (*2*) The fit of the crystal structure of MLT (Terwilliger and Eisenberg, 1982a; Terwilliger and Eisenberg, 1982b) (PDB coördinates 2mlt) with the plane of the Pro^{14} kink normal to the bilayer. The fit is far outside the experimental uncertainty. (*3*) The fit of the crystal structure of MLT with the plane of the Pro^{14} kink parallel to the membrane plane. Although the model falls near the edge of the experimentally determined distribution, it cannot be more than a minor constituent of the dynamic ensemble of conformations comprising the MLT transbilayer distribution.

9,10 position of the *sn*-2 chain, as described in detail elsewhere (Wiener and White, 1991c; Hristova and White, 1998). Briefly, the experimental structure factors $f(h)$ from a given experiment depend upon the amount of sample in the beam, precise geometry of the sample–beam interaction, x-ray beam intensity, and other experimental conditions. The true (absolute) structure factors, $F(h)$, are determined solely by the scattering factor of the unit cell. The experimental structure factors are related to the true structure factors by $f(h) = KF(h)$ in which K is the instrumental constant. Fourier reconstructions of bilayer scattering-length or electron density profiles yield only arbitrary fluctuations of scattering density along the bilayer normal if the average scattering length density of the unit is not accounted for, and whether $f(h)$ rather than $F(h)$ is used. Determination of the instrumental constant allows one to relate the scattering profiles obtained in diffraction experiments to the actual contents and molecular packing of the bilayer unit cell. To do this, one must determine the true mean value of the scattering profile using the composition of the unit cell and calibrate the fluctuations around this mean value based upon difference structures of Br-labeled and unlabeled DOPC bilayers (Franks et al., 1978; Wiener and White, 1991c; Hristova and White, 1998). (It is these difference structures that disclose the transbilayer distribution of Br-labeled double-bonds.) The absolute scattering lengths are easily computed from knowledge of the mole fraction of Br-labeled DOPC in the bilayer and known scattering length of Br. This serves to calibrate the amplitude of the fluctuations on the absolute scale.

Data scaling and phasing

We scaled the diffracted intensities by gathering complete x-ray data sets for at least six OBPC:DOPC mole fractions ranging from 0 to 1. This procedure, used for both MLT and Q25C, is equivalent to six experimental determinations of the structure factors, but with several bonuses. It reduces experimental uncertainties, averages out random error, and assures that OBPC is isomorphous with DOPC in the presence and absence of the peptide. Isomorphous behavior is proven if the measured structure factors are linear functions of the mole fraction of OBPC. Wiener and White (1991c) have described in detail a procedure for scaling multiple data sets that involves, in simple terms, rescaling the structure factors so that the

data sets are described by a set of internally consistent experimental constants. One result of the procedure, automated by means of computer programs, is good estimates of the experimental uncertainties of the structure factors, which is necessary for establishing the value of the so-called self-R-factor (see below). Another result is that the phases of the structure factors, at all OBPC mole fractions, are established unequivocally (Wiener and White, 1991c; Hristova et al., 1999).

Perturbed-bilayer models

The structure of the perturbed bilayer in the experiments with MLT was estimated (Hristova et al., 1999) from the measured changes in the parameters of the bromine distribution A_{Br} and Z_{Br} and the Bragg spacing d. The bromine distribution reports the distribution of double bonds in DOPC bilayers and provides information about the physical state of the hydrocarbon core (Hristova and White, 1998). The comparison of the bromine distributions with and without peptide reveals the changes in the hydrocarbon region that occur due to peptide insertion (Hristova et al., 1999). We created several bilayer models based upon the measured changes in d-spacing or Z_{Br}, and judged their adequacy against the experimental data in the structure refinement process. Only those models with $R < R_{self}$ (see below) were retained. We found that satisfactory models could be produced in only two ways. In the first, called Model A, only the positions of the lipid components were scaled according to the measured change in Bragg spacings (see Hristova et al., 1999). That is, the Gaussian positions of the Wiener and White (1992) structure were simply scaled by $d_{DOPC+MLT}/d_{DOPC}$. The widths were not changed. In the second, called Model B, good fits were obtained by additionally scaling the widths in accordance with the slight increase in the bromine width distribution in the presence of MLT. The methods for evaluating the quality of the structure refinement have been described in detail (Hristova et al., 1999).

The number of structure factors required to describe the perturbed bilayer profile is determined by the sum of the structure factors resulting from the Gaussian distributions, and also careful consideration of experimental uncertainty and signal-to-noise ratios. We typically consider values as high as $h = 8$, the number observed for the neat bilayer. But an interesting thing happens when the structure factor contributions of the peptide are added to obtain the model peptide + bilayer structure factors for comparing to the observed structure factors: The number of structure factors observable, h_{max}, decreases because of the smoothing effect of the broad peptide distribution! We have discussed this phenomenon in quantitative detail elsewhere (Hristova et al., 1999). Because of it, the difference in number of structure factors between the neat and peptide-containing structure factors is automatically reconciled, physically. A practical problem remains, however. Upon adding the structure factors of the MLT Gaussian distribution (below) to the perturbed-bilayer structure factors, we have only five experimental peptide + bilayer structure factors for carrying out the optimization of the MLT Gaussian. We resolve the problem by simply using the first five structure factors of the model bilayer, and ignoring the higher ones. When we follow this protocol, we invariably find that the higher-order structure factors produced by the model bilayer + MLT Gaussian are predicted to be below the limits of experimental detectability, as discussed by Hristova et al. (1999).

Determination of Gaussian parameters for the melittin distribution

The Gaussian parameters of the MLT transbilayer distribution were determined by nonlinear least-square fitting of the calculated structure factors to the experimental ones (Hristova et al., 1999). For a particular model bilayer, the refinement computation finds the optimal position Z_{MLT} and width A_{MLT} of the peptide transbilayer distribution. For each cycle of the computation, the structure factors of the peptide distribution were added to the fixed structure factors of the bilayer model. These summed structure factors were then compared to the observed structure factors of the DOPC/MLT complex by means of the crystallographic R-factor.

Peptide modeling

The most realistic approach to modeling the peptide would be to produce an ensemble of conformations in a bilayer environment by molecular dynamics simulations, but this approach is presently impractical. We therefore adopted a simpler method that allowed us to explore a reasonable range of peptide backbone and sidechain conformations. For a particular peptide conformation, each atom (a) was represented in the z-axis projection by a Gaussian scattering distribution whose $1/e$-halfwidth A_a was related to the atom's B-factor. All atoms were assigned the same B-factor during the refinement procedure, for two reasons. First, we did not have a sufficient number of structure factors to vary the B-factors of, say, individual residues. Second, because of the very high thermal disorder of the bilayer, there is no reason to expect significant differences in B-factors among the sidechains. As discussed below, we accept only those models whose average B-factor is within the range of B-factors of the lipid components.

The peptide model-building step was implemented by generating a library of peptide structures using molecular dynamics simulations whose positions and orientations in the bilayer were optimized by refinement of the calculated structure factors of the bilayer/peptide complex against the observed structure factors. The primary refinement variables used were the position and tilt of the peptide axis and the average crystallographic Debye temperature factor (B) of the peptide's atoms. The B-factor is a measure of the amplitude of the thermal fluctuations of an atom around its mean position (Warren, 1969). By "average" B, we mean that a single B-factor was applied to all atoms (above). We assumed that the transbilayer Gaussian envelope of the whole peptide could be obtained by summing the Gaussian scattering-length densities of the individual atoms and that the most likely atomic B-factors would be those that were close to the B-factors of lipid component groups. The latter assumption is reasonable because the conformational flexibility of the peptide must surely reflect the thermal motion of its surroundings, i.e., the fluid bilayer. This assumption provided the basis for choosing the most likely peptide conformations from the library of peptide structures.

The Gaussian obtained in the determination stage was thus used in a second minimization routine to obtain the optimum average B-factor for a particular structural model. If the calculated B-factors were of the order of the B-factor for the glycerol moiety (Hristova et al., 1999) (78 Å^2) or higher (but $<$200 Å^2), the conformation was considered consistent with the data. A library of MLT conformations was created with the software package Insight II (Biosym Technologies, San Diego, CA). After minimization, 1 ps molecular dynamics simulations were carried out at 300 K to produce a range of sidechain conformations. The projections of the atom coordinates along the bilayer normal defined the centers of the transbilayer distributions of the atoms. The average of these projections defined the center of the helix transbilayer distribution. The widths of the atom distributions were characterized by a Gaussian with $1/e$-halfwidth A, given by $A^2 = A_c^2 + A_a^2$, where A_c is the covalent radius of the atom, and A_a is the thermal atomic $1/e$-halfwidth, which is a measure of the thermal motion of the atom in the fluid bilayer. The value of A_a is related to the crystallographic B-factor according to $B = 4\pi^2 A_a^2$.

Refinement computations

The computations used nonlinear minimization of R using the standard Levenberg–Marquardt algorithm (Bevington, 1969; Press et al., 1989). Only those solutions were accepted whose R-factors were smaller than the so-called "self" R (R_{self}) of the observed structure factors. R_{self} is defined (Wiener and White, 1991b) as $R_{self}^2 = \Sigma_h (\sigma(h))^2/\Sigma_h (F^*(h))^2$, where the $\sigma(h)$ are the uncertainties in the determination of the structure factors

F^*(h). R_{self} measures, in essence, the total experimental uncertainty of the observed structure factors after scaling (Wiener and White, 1991b). The value of R_{self} was 6.0×10^{-2} for the experiments reported here.

Error analysis

The robustness of the fits and the uncertainties in Z_{MLT} and A_{MLT} for the MLT distribution (Step 3) were determined using the Monte Carlo sampling procedure of Wiener and White (1991a,b). This procedure is based upon the fact that each structure factor has an experimental uncertainty $\sigma(h)$ that can be used to define a normal distribution for each structure factor $F(h)$. In simple terms, a Box–Muller algorithm (Ross, 1989) seeded with a random number is used to generate sets of "mock" structure factors from the observed $F(h)$ and $\sigma(h)$. The mean and standard deviation of these mock sets will match those of the observed data. Although each set of mock data represents a statistically acceptable combination of structure factor amplitudes, each set will yield slightly different values for the parameters obtained in the refinement. The mean values and standard deviations of the collection of parameters describe the most likely values of the parameters and their uncertainties. If all of the sets of mock data lead to a convergence of the refinement, the fits can be considered robust. The error ranges noted in the figures and tables were obtained in this way.

RESULTS AND DISCUSSION

Disposition of melittin in DOPC bilayers

The absolute per-lipid scale bilayer profiles determined for pure DOPC (Wiener and White, 1992; Hristova et al., 1999) and DOPC + 1 mol% MLT are shown in Fig. 1 *A* and the corresponding structure factors in Table 1. The half-unit cell contents, required for the absolute scaling, are 5.4 waters per lipid in the absence of MLT and 5.6 waters, 0.01 MLT, and 0.06 acetyl counterion per lipid in the presence of MLT. (Six acetyl counterions remain associated with MLT after freeze-drying, as determined by NMR [data not shown]). On a volume-fraction basis, MLT plus the acetyl counterions accounted for 2.75% of the unit-cell volume. Even casual examination of the two profiles in Fig. 1 *A* discloses a highly significant increase in scattering density in the headgroup region of the bilayer when MLT is present. In the central region of the DOPC/MLT profile, corresponding to the bilayer HC core, the changes caused by MLT are barely outside experimental uncertainty (*dotted lines*). The MLT-induced bilayer perturbations were small enough to allow models for the perturbed bilayer to be generated from the unperturbed bilayer structure (Wiener and White, 1992) by the simple scaling procedure (Hristova et al., 1999) described in Methods. The profile of one model is shown in Fig. 1 *C* (*blue curve*) and a partial set of component distributions in Fig. 2 *A*. The packing constraints on the bilayer are not apparent in such distributions because the contents of the unit cell are projected onto the bilayer normal, causing the component groups to overlap. In three-dimensions, however, the component groups are excluded from each others' volumes (discussed in Hristova et al., 1999).

Starting with the perturbed-bilayer models and superposed Gaussians for the MLT transbilayer distribution, the positions ($\pm Z_{MLT}$) and widths (A_{MLT}) of MLT distributions were obtained by nonlinear least-squares fitting in reciprocal space. Parameters resulting from the two different bilayer models, A and B (above), are shown in Table 2. Fig. 1 *C* shows the five-order Fourier reconstruction of the profiles of the model bilayer (*blue curve*), MLT (*violet curve*), and the composite of the two (*red curve*). The excellent quality of the refinement is apparent from the tight overlap of the composite with the experimentally determined profile (*black dashed line*). The best estimates for the MLT Gaussian parameters are $Z_{MLT} = 17.5(\pm 0.2)$ Å and $A_{MLT} = 4.3(\pm 0.4)$ Å, obtained by averaging the values in Table 2. The MLT distribution is superimposed on the component distributions of the perturbed-bilayer model in Fig. 2 *A*. The center of the distribution is very nearly the same as that of the glycerol moiety of the DOPC bilayer. OCD measure-

TABLE 1 Structural data for DOPC/melittin and DOPC/Q25C bilayers

	DOPC*	DOPC + melittin	DOPC + Q25C
d (Å)†	49.1 ± 0.30	48.2 ± 0.50	48.2 ± 0.50
Z_{BR} (Å)‡	7.97 ± 0.27	7.56 ± 0.05	7.71 ± 0.04
A_{BR} (Å)§	4.96 ± 0.62	5.26 ± 0.28	5.65 ± 0.15
F_1¶	−43.95	−50.46 ± 2.9	−45.79 ± 2.1
F_2	−0.52	1.17 ± 0.07	2.15 ± 0.31
F_3	5.15	8.31 ± 0.6	7.00 ± 0.32
F_4	−11.97	−15.09 ± 1.2	−15.47 ± 0.76
F_5	3.38	4.06 ± 0.3	4.07 ± 0.4
F_6	−2.47	n.o.‖	n.o.
F_7	2.03	n.o.	n.o.
F_8	−2.24	n.o.	n.o.

*Data taken from Wiener and White (1991c).
†Bragg spacing ± SD.
‡Center of bromine-labeled double-bond distribution.
§1/*e*-Halfwidth of bromine-labeled double-bond distribution.
¶Absolute (per-lipid) x-ray structure factors. Scattering-length density profiles $\rho^*(z)$ (e.g., Figs. 1 and 2) may be reconstructed from $\rho^*(z) = \rho_0^* + (2/d)\,\Sigma_{h=1}^{N} F_h \cdot 10^{-12} \cos(2\pi hz/d)$ where d is in cm, the F_h are read from the Table, and ρ_0^* is the average per-length scattering density of the unit cell (see Jacobs and White, 1989; Hristova et al., 1999). Because $\rho^*(z)$ has dimensions of length/length, it is dimensionless, but it has magnitude of 10^{-4} arising from $10^{-12}/d$ in the equation. See Appendix. The phases are the same as for DOPC + Ac-18A-NH_2.
‖Not observable, see text.

TABLE 2 Gaussian parameters of the melittin distribution for four different model bilayers

Model Bilayer*	Z_{MLT} (Å)†	A_{MLT} (Å)‡	$R \times 10^2$§
A	17.6 ± 0.2	4.01 ± 0.4	2.5
B	17.4 ± 0.2	4.56 ± 0.4	2.6

*Melittin counterions are included with the water distribution.
†Center of melittin in DOPC scattering distribution bilayers.
‡1/*e* Half-width of the scattering distribution of melittin.
§*R*-factor, see Methods. The value of R_{self}, 6.0×10^{-2}. See discussion in Methods.

ments on MLT in oriented DOPC multilayers obtained under experimental conditions identical to those of the diffraction experiments showed that MLT was helical and oriented parallel to the bilayer plane (below). The center of the observed distribution therefore corresponds to the location of the helix axis and the width of the distribution approximately to the average diameter of the helix, ~9 Å. Figure 2 *A* shows, then, that the surface of the MLT helix extends to about the depth of the DOPC double bonds.

The most likely helical conformations of MLT that account for the observed distribution were determined by first creating a library of helical conformations derived from the NMR models of Dempsey and Butler (1992) and Okada et al. (1994) using methods previously described (Hristova et al., 1999). Because both studies indicated that the last four residues (KRQQ) lack secondary structure in membranes, we included this feature in all models. The structure factors of these models were evaluated against the structure factors of the experimentally determined MLT Gaussian (above) by determining the average *B*-factors required for a satisfactory fit. Acceptable models were those with average *B*-factors falling between 70 and 200 Å^2, which are characteristic of fluid bilayers (Hristova et al., 1999). One of many possible models that is consistent with the experimental data is shown in Fig. 2 *B*[1] (*red dashed curve*) along with the experimentally determined distribution (*solid black curve*). For this model, $B = 140$ Å^2. The excellent quality of the model is obvious from the fact that its distribution is well within the experimental uncertainty of the observed distribution (*black dashed curves*). Only those conformations that were highly helical and oriented parallel to the bilayer surface satisfied the experimental distribution, consistent with OCD measurements (below).

We specifically examined the possibility that MLT in the conformation observed in the crystal could explain our diffraction results. The crystallographic model of MLT oriented with the plane of the Pro^{14} kink normal to the membrane plane, as proposed by Terwilliger et al. (1982), did not provide a satisfactory fit to the observed distribution (Fig. 2 *B*[2]) with $B = 140$ Å^2. Nor did orientation of the kink parallel to the bilayer plane (Fig. 2 *B*[3]). The kink-parallel crystallographic conformation is thus, at best, a minor constituent of the ensemble of conformations represented by the observed MLT distribution. But we could not arrive at satisfactory fits of the crystallographic structures unless the average *B*-factors of the structures were fixed at nearly 0. This in itself shows that the crystallographic models do not describe the conformation of MLT in fluid bilayers.

Bilayer perturbations due to monomeric mellittin

The introduction of MLT into the DOPC bilayer caused the Bragg spacing *d* to decrease and the brominated double-bond position Z_{Br} to shift toward the bilayer center with a slight increase of its 1/*e*-halfwidth A_{Br} (Table 1). The distributions of the DOPC double bonds in the presence and absence of MLT, as reported by Br at the 9,10 positions of the *sn*-2 chain of OBPC, are shown in Fig. 3 *A* (*blue curve* and *dashed black curve*, respectively). These changes show that monomeric MLT has a remarkably modest effect on the structure of the DOPC bilayer at low concentrations. And so does the amphipathic helical peptide Ac-18A-NH$_2$ (Hris-

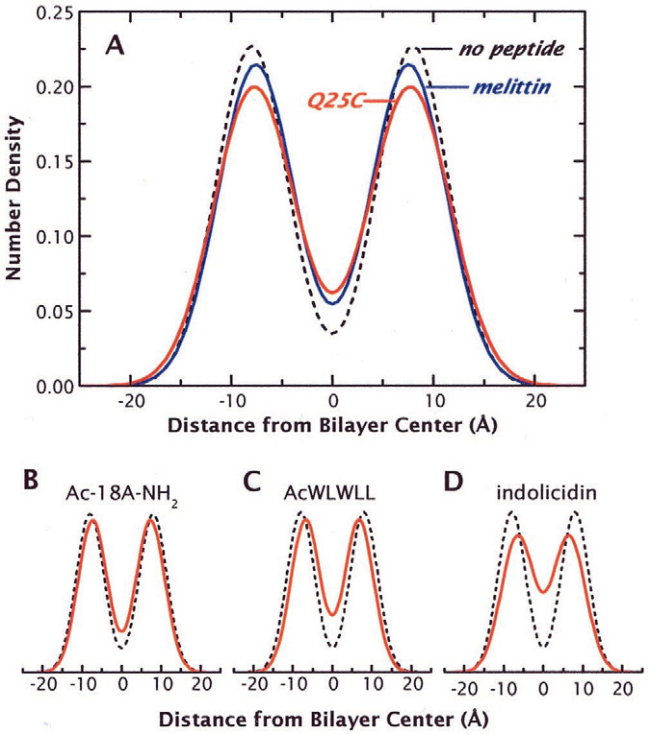

FIGURE 3 Experimentally determined distributions of brominated double bonds in the neat DOPC bilayer (*black dashed lines*) and in DOPC bilayers containing peptides (*solid curves*) with regular and nonregular secondary structure. Here the distributions are described in "composition space" by using densities such that the total area under the curves equals 4, corresponding to the total number of double bonds in a unit cell (see Wiener and White, 1991b). Compared to peptides without regular secondary structure, such as Ac-WLWLL and indolicidin, amphipathic helices induce surprisingly modest changes in the double-bond distribution. (*A*) The distributions associated with the monomer MLT (*blue curve*) and the dimer Q25C (*red curve*). The volume fraction of the unit cell occupied by either MLT was 2.75%. The dimeric form of MLT induces further widening of the double-bond distribution and generally increases bilayer perturbations of all sorts (Fig. 1 *B*). (*B*) Distribution of the double bonds (*red curve*) in the presence of 5 mol% of the amphipathic helix Ac-18A-NH$_2$, corresponding to a unit-cell volume fraction of 10.6%. It is very similar to the distribution seen for MLT despite its much higher concentration. Data taken from Hristova et al. (1999). (*C*) Double-bond distribution of DOPC determined in the present study for the unstructured pentapeptide (Wimley and White, 1996) AcWLWLL (unit-cell volume fraction 6.7%). (*D*) Double-bond distribution determined in the present study for the antimicrobial peptide indolicidin (Selsted et al., 1992; Ladokhin et al., 1997b, 1999) that lacks regular secondary structure (unit-cell volume fraction 7.6%). Even though the volume fraction concentrations of AcWLWLL and indolicidin are smaller than for Ac-18A-NH$_2$, the perturbations are dramatically larger.

tova et al., 1999), a model for apolipoprotein A-I that is known for its ability to completely solubilize bilayer phases at high concentrations (Mishra et al., 1994). The MLT and 18A results together thus raise the possibility that very small changes in Z_{Br} and A_{Br} may be peculiar to amphipathic helices at bilayer interfaces, at least a low concentrations.

Figure 3 *B* shows the notably small effect of 5 mol% Ac-18A-NH_2, corresponding to a unit-cell volume fraction of 10.6%. The surprising noninvasive behavior of monomeric amphipathic helices becomes apparent when the helix-induced perturbation of the double-bond distribution is compared to the changes induced by two, small unstructured peptides: the pentapeptide (Wimley and White, 1996) AcWLWLL (10 mol%; 6.7% unit-cell volume-fraction) and the 13-residue antimicrobial peptide indolicidin (Selsted et al., 1992; Ladokhin et al., 1997b, 1999) (5 mol%; 7.6% unit-cell volume-fraction). The most significant features of the perturbations in these two cases are the broadening and the substantial shift of the double-bond distribution toward the bilayer center (Fig. 3, *C* and *D*). These bilayer perturbations are so large that the construction of models from the component distributions of the neat DOPC bilayer are precluded. It is thus clear that, at low concentrations, amphipathic helices that have the ability to solubilize bilayers at high concentrations fit nicely into the bilayer interface with few bilayer perturbations beyond those expected from slight increases in the area per lipid.

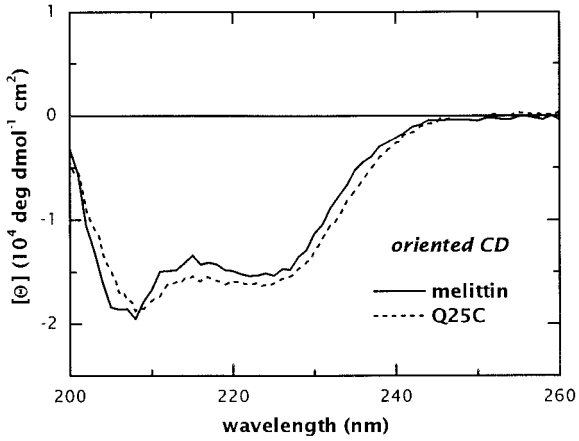

FIGURE 4 Oriented circular dichroism spectra for MLT and Q25C. Both spectra are characteristic of α-helices oriented parallel to the bilayer surface. The monomeric-equivalent concentrations of the two MLT forms are virtually identical in the oriented multilayers, based upon measurements of optical density. Notice that the CD spectra are nearly identical, allowing for experimental uncertainties. The OCD measurements of MLT are difficult at the very low, 1 mol% concentration used because of the very low signal-to-noise. This makes it hard to establish the average baselines accurately, and, consequently, the absolute magnitudes of the ellipticity. The helicity of ~40% computed at 222 nm from these data is thus a rough estimate, at best. The significant experimental observation is the similarity of the shapes of the curves, which depend strongly on the orientation of the helix axis with respect to the optical axis.

Bilayer perturbations due to dimeric mellittin

OCD measurements of dimeric Q25C in DOPC bilayers gave spectra virtually identical with those of MLT under otherwise identical conditions, as shown in Fig. 4. Q25C therefore had high helicity and was oriented parallel to the bilayer plane. Nevertheless, the structure of DOPC/Q25C bilayers is quite different from DOPC/MLT bilayers. The profiles for DOPC with and without dimeric Q25C are shown in Fig. 1 *B* (*red* and *blue curves*, respectively). The effect of Q25C on the double-bond distribution as reported by the OBPC bromine labels is shown in Fig. 3 *A* (*red curve*). At the same monomer-per-lipid concentration used for monomeric MLT, the Q25C dimer caused a significant increase in A_{Br} compared to the monomer. Table 1 shows that the values of Z_{Br} and A_{Br} are statistically different for the monomer and dimer, even though not visually striking in Fig. 3 *A*. Although the shift in Z_{Br} toward the bilayer center was smaller for Q25C than for MLT, the overall perturbation was quite large. The Q25C perturbation is so large that it entirely precludes successful modeling of the perturbed bilayer. That is, no simple rescaling procedure ever resulted in models whose structure factors were within experimental uncertainty. More visually revealing is the dramatic change in the bilayer profile near the center of the bilayer. A comparison of Fig. 1, *A* and *B* shows that the Q25C perturbations affect the entire bilayer rather than just the double-bond distribution. Differences in the bilayer profiles caused by added peptide arise from both the added scattering density of the peptide and the scattering-density changes of the bilayer due to lipid rearrangements. Studies using specific deuteration and neutron diffraction will be necessary to understand the nature of the perturbations. We expect the perturbations to depend strongly on concentration. The results reported here for MLT and Q25C at low concentrations provide a reference point for such measurements.

CONCLUSIONS

Our results show that MLT in fluid bilayers is unlikely to prefer the conformation observed in the crystal structure. One model that is consistent with our data and NMR data (Dempsey and Butler, 1992; Okada et al., 1994) is a generally helical conformation encompassing the first 22 residues and an extended conformation running roughly parallel to the bilayer plane for the last four residues. Of course, MLT must adopt many different conformations represented as an ensemble average in the diffraction experiment. The image obtained in our x-ray experiments is one-dimensional, along the bilayer normal, and thus does not contain information about the organization of the peptides in the bilayer plane, especially the nature of the association of the monomers comprising Q25C. Also, without specific heavy-atom labeling of the peptide, we can say nothing about the

relative depths of different MLT residues in the bilayer, because orientations obtained via rotation of the molecule around the helix axis are indistinguishable. In the model of Dempsey and Butler (1992), Pro^{14} is positioned roughly at the same depth in the bilayer as the helix axis. A kink may exist in the plane of the bilayer, but an orientation of the kink-plane normal to the bilayer surface (Fig. 3 *B*) is extremely unlikely.

Although the disposition of MLT can change with hydration, monomeric MLT in fully hydrated bilayers is parallel to the bilayer plane (Altenbach and Hubbell, 1988; Altenbach et al., 1989; Frey and Tamm, 1991; Dempsey and Butler, 1992) as observed here for lower hydrations. We have already shown that the structure of the pure DOPC bilayer does not change substantially over a wide range of hydrations (Hristova and White, 1998). The results reported here are thus very likely to be true at full hydration, especially because the conformation of MLT is consistent with that determined by NMR at full hydration. They also demonstrate that absolute-scale lamellar diffraction is an important tool for studying the disposition of peptides in bilayers.

Considering the highly destabilizing effect of amphipathic helices at high concentrations, we expected both MLT and Ac-18A-NH_2 to have a far greater effect on bilayer structure, even at the low concentrations used here. The changes in bilayer structure seen, however, are stunningly small. This observation alone strongly implicates helix association as a necessary precursor to bilayer destabilization. The increased bilayer perturbation of Q25C at low concentration is apparently a harbinger of destabilization. As MLT or Q25C concentrations are increased, we expect to observe major changes in bilayer organization and, ultimately, reorientation of the helices into a transmembrane configuration. Indeed, early neutron diffraction studies (Strom et al., 1983; Bradshaw et al., 1994) on MLT at concentrations of 5–10 mol% suggested such an orientation, and more recent NMR studies (Smith et al., 1994; Naito et al., 2000) have proven it. In the course of the present experiments, we found by OCD that MLT began reorienting at ~4 mol%. Crucial questions that remain to be answered are how the lipids adapt to helices as peptide concentration increases and how these adaptations may lead toward destabilization of the membrane-parallel orientation of helices, and ultimately to complete destabilization of the bilayer at high peptide concentrations.

Besides being important in pore formation, helix association also appears to be important in membrane fusion. This is because the helical bundle has emerged as the principal motif of fusion peptides. These bundles are generally envisioned as having a membrane-parallel surface-bound state near the time of the membrane-destabilizing fusion event (Skehel and Wiley, 1998). A general principle arising from studies of both MLT and fusion peptides is that helix multimers have a destabilizing effect on membrane integrity. The structural approach used here may thus provide important insights into membrane fusion when applied to helical-bundle fusion peptides.

APPENDIX: THE PER-LIPID ABSOLUTE SCALE

An x-ray profile on an absolute scale is a measure of electron density (number n per unit volume, n/cm^3) as a function of position in the unit cell. For small-angle diffraction, the "strength" of the scattering of X-rays by electrons is measured by the scattering length b (cm), which is simply proportional to n: $b = n \cdot mc^2/e^2$, where c is the speed of light, m is electron mass, and e is electron charge (Woolfson, 1970). One can thus also describe x-ray profiles in terms of scattering-length density ρ, which has units of $b/\text{cm}^3 = \text{cm}^{-2}$. As noted in Materials and Methods, we have historically used scattering-length density rather than electron density because it is more convenient when combining x-ray and neutron diffraction data.

On the true absolute scale, the scattering-length density is given by

$$\rho(z) = \rho_0 + \frac{2}{d}\sum_{\text{h}} F(h)\cos\left(\frac{2\pi hz}{d}\right), \qquad \text{(A1)}$$

where the $F(h)$ are the absolute-scale structure factors and ρ_0 is the average scattering-length density of the unit cell given by

$$\rho_0 = \frac{2}{Sd} b_{\text{uc}}. \qquad \text{(A2)}$$

In Eq. A2, S is the cross-sectional area of the unit cell, d is the Bragg Spacing, and b_{uc} the total scattering length of the half-unit cell contents (consisting of a single lipid, waters, and a portion of the peptide). To avoid needing to know S, we have defined the scattering-length density on the per-lipid scale by multiplying both sides of Eq. A1 by S to arrive at $\rho^*(z) = \rho(z) \cdot S$, which is dimensionless (see Jacobs and White, 1989).

The per-lipid scale has two advantages. First, the experimental uncertainties of per-lipid scale profiles are reduced compared to profiles on the true absolute scale because the uncertainties of S are avoided. Inclusion of the uncertainty of S will significantly broaden the error bands shown in Fig. 1 *A*, causing the position of the peptide to be less certain. Second, $\rho^*(z)$ is more sensitive to the presence of the peptide than $\rho(z)$; its amplitude is determined almost entirely by the number of electrons in the unit cell, rather than the number per unit volume. This is true because the Bragg spacing typically changes by only about 2% upon the addition of peptide (Table 1), causing $\rho^*(z) \sim \text{constant} \times b_{\text{uc}}$. This can be seen more clearly by considering the effect of MLT in our experiments.

Based upon partial specific volumes of MLT, computed from the data of Makhatadze et al. (1990), and the hydrated phosphocholine group (Wiener and White, 1992), the electron densities are $(1536/3736\ \text{Å}^3) = 0.41\ e/\text{Å}^3$ and $(218/498\ \text{Å}^3) = 0.44\ e/\text{Å}^3$, respectively. This is consistent with the findings of MacNaughtan et al. (1985), who observed a drop in electron density relative to the lipid headgroups for cytochrome c bound to the surface of cerebroside sulfate/cholesterol bilayers. It is apparent that 1 mol% of MLT in the DOPC headgroup region would be difficult, if not impossible, to detect using an $e/\text{Å}^3$ scale. The situation for the per-lipid scale is dramatically different. The addition of 0.01 MLT increases the number of electrons in the headgroup region from 218 to 233, an increase of ~7%. Our results show that this increase is easily detected.

In earlier papers from our laboratory, we used the nomenclature "Scattering Density: $\rho(z) \cdot S \cdot 10^4$" to describe scattering density on bilayer-profile plots. But we now use "Scattering Density per Lipid $\times 10^4$," introduced in our paper concerned with the disposition of the 18A peptide in lipid bilayers (Hristova et al., 1999). The factor of 10^4 applied to a dimensionless quantity at first sight seems meaningless. Here is the explanation. We use Ångströms for lengths and square Ångströms for areas, so that, in centimeters, $\rho_0 \cdot S$ is on the order of $10^{-12}/10^{-8} = 10^{-4}$ (dimen-

sionless). Thus, the per-lipid scattering density values shown in our plots are multiplied by 10^4 to indicate that the numbers read from the ordinate should be multiplied by the reader by 10^{-4} for use in computations. Because the values of the structure factors we report take these issues into account, we include this factor of 10^4 in bilayer profiles.

The need for the 10^{-4} factor is also apparent from the scattering length conversion factor mc^2/e^2 (above), which has numerical value 0.282×10^{-12} cm, or 0.282×10^{-4} Å. From Eq. A2, for a unit cell measured in Å containing n_{uc} electrons, the scattering density per lipid is $n_{uc}(mc^2/e^2)/d$ or $0.282(n_{uc}/d) \times 10^{-4}$.

This research was supported in part by a grant from the National Institutes of Health (GM-46823). We thank Drs. William Wimley and Alexey Ladokhin for many helpful conversations.

REFERENCES

Altenbach, C., W. Froncisz, J. S. Hyde, and W. L. Hubbell. 1989. Conformation of spin-labeled melittin at membrane surfaces investigated by pulse saturation recovery and continuous wave power saturation electron paramagnetic resonance. *Biophys. J.* 56:1183–1191.

Altenbach, C., and W. L. Hubbell. 1988. The aggregation state of spin-labeled melittin in solution and bound to phospholipid membranes: evidence that membrane-bound melittin is monomeric. *Proteins.* 3:230–243.

Bachar, M., and O. M. Becker. 1999. Melittin at a membrane/water interface: effects on water orientation and water penetration. *J. Chem. Phys.* 111:8672–8685.

Bachar, M., and O. M. Becker. 2000. Protein-induced membrane disorder: a molecular dynamics study of melittin in a dipalmitoylphosphatidylcholine bilayer. *Biophys. J.* 78:1359–1375.

Baumann, G., and P. Mueller. 1974. A molecular model of membrane excitability. *J. Supramol. Struc.* 2:538–557.

Bernèche, S., M. Nina, and B. Roux. 1998. Molecular dynamics simulation of melittin in a dimyristoylphosphatidylcholine bilayer membrane. *Biophys. J.* 75:1603–1618.

Bevington, P. R. 1969. Data Reduction and Error Analysis for the Physical Sciences, McGraw-Hill Book Company, New York.

Bradshaw, J. P., C. E. Dempsey, and A. Watts. 1994. A combined x-ray and neutron diffraction study of selectively deuterated melittin in phospholipid bilayers: effect of pH. *Mol. Membr. Biol.* 11:79–86.

DeGrado, W. F., G. F. Musso, M. Lieber, E. T. Kaiser, and F. J. Kézdy. 1982. Kinetics and mechanism of hemolysis induced by melittin and by a synthetic melittin analogue. *Biophys. J.* 37:329–338.

Dempsey, C. E. 1990. The actions of melittin on membranes. *Biochim. Biophys. Acta.* 1031:143–161.

Dempsey, C. E., and G. S. Butler. 1992. Helical structure and orientation of melittin in dispersed phospholipid membranes from amide exchange analysis in situ. *Biochemistry.* 31:11973–11977.

Fox, R. O. Jr., and F. M. Richards. 1982. A voltage-gated ion channel model inferred from the crystal structure of alamethicin at 1.5-Å resolution. *Nature (London).* 300:325–330.

Franks, N. P., T. Arunachalam, and E. Caspi. 1978. A direct method for determination of membrane electron density profiles on an absolute scale. *Nature (London).* 276:530–532.

Franks, N. P., and Y. K. Levine. 1981. Low-angle x-ray diffraction. *In* Membrane Spectroscopy, E. Grell, editor. Springer-Verlag, Berlin. 437–487.

Frey, S., and L. K. Tamm. 1991. Orientation of melittin in phospholipid bilayers: a polarized attenuated total reflection infrared study. *Biophys. J.* 60:922–930.

Habermann, E. 1972. Bee and wasp venoms. *Science.* 177:314–322.

Hall, J. E., I. Vodyanoy, T. M. Balasubramanian, and G. R. Marshall. 1984. Alamethicin: a rich model for channel behavior. *Biophys. J.* 45:233–247.

Hristova, K., and S. H. White. 1998. Determination of the hydrocarbon core structure of fluid dioleoylphosphocholine (DOPC) bilayers by x-ray diffraction using specific bromination of the double-bonds: effect of hydration. *Biophys. J.* 74:2419–2433.

Hristova, K., W. C. Wimley, V. K. Mishra, G. M. Anantharamaiah, J. P. Segrest, and S. H. White. 1999. An amphipathic α-helix at a membrane interface: a structural study using a novel x-ray diffraction method. *J. Mol. Biol.* 290:99–117.

Jacobs, R. E., and S. H. White. 1989. The nature of the hydrophobic binding of small peptides at the bilayer interface: implications for the insertion of transbilayer helices. *Biochemistry.* 28:3421–3437.

John, E., and F. Jähnig. 1991. Aggregation state of melittin in lipid vesicle membranes. *Biophys. J.* 60:319–328.

Katsu, T., C. Ninomiya, M. Kuroko, H. Kobayashi, T. Hirota, and Y. Fujita. 1988. Action mechanism of amphipathic peptides gramicidin S and melittin on erythrocyte membrane. *Biochim. Biophys. Acta.* 939: 57–63.

Ladokhin, A. S., M. E. Selsted, and S. H. White. 1997a. Sizing membrane pores in lipid vesicles by leakage of co-encapsulated markers: pore formation by melittin. *Biophys. J.* 72:1762–1766.

Ladokhin, A. S., M. E. Selsted, and S. H. White. 1997b. Bilayer interactions of indolicidin, a small antimicrobial peptide rich in tryptophan, proline, and basic amino acids. *Biophys. J.* 72:794–805.

Ladokhin, A. S., M. E. Selsted, and S. H. White. 1999. CD spectra of indolicidin antimicrobial peptides suggest turns, not polyproline helix. *Biochemistry.* 38:12313–12319.

Ladokhin, A. S., and S. H. White. 1999. Folding of amphipathic α-helices on membranes: energetics of helix formation by melittin. *J. Mol. Biol.* 285:1363–1369.

Lin, J.-H. and A. Baumgärtner. 2000. Adsorption of melittin to a lipid bilayer: a molecular dynamics study. *J. Mol. Liquids.* 84:89–98.

MacNaughtan, W., K. A. Snook, E. Caspi, and N. P. Franks. 1985. An x-ray diffraction analysis of oriented lipid multilayers containing basic proteins. *Biochim. Biophys. Acta.* 818:132–148.

Makhatadze, G. I., V. N. Medvedkin, and P. L. Privalov. 1990. Partial molar volumes of polypeptides and their constituent groups in aqueous solution over a broad temperature range. *Biopolymers.* 30:1001–1010.

Matsuzaki, K., S. Yoneyama, and K. Miyajima. 1997. Pore formation and translocation of melittin. *Biophys. J.* 73:831–838.

Mishra, V. K., M. N. Palgunachari, J. P. Segrest, and G. M. Anantharamaiah. 1994. Interactions of synthetic peptide analogs of the class A amphipathic helix with lipids: evidence for the snorkle hypothesis. *J. Biol. Chem.* 269:7185–7191.

Naito, A., T. Nagao, K. Norisada, T. Mizuno, S. Tuzi, and H. Saito. 2000. Conformation and dynamics of melittin bound to magnetically oriented lipid bilayers by solid-state ^{31}P and ^{13}C NMR spectroscopy. *Biophys. J.* 78:2405–2417.

Okada, A., K. Wakamatsu, T. Miyazawa, and T. Higashijima. 1994. Vesicle-bound conformation of melittin: transferred nuclear Overhauser enhancement analysis in the presence of perdeuterated phosphatidylcholine vesicles. *Biochemistry.* 33:9438–9446.

Press, W. H., B. P. Flannery, S. A. Teukolsky, and W. T. Vetterling. 1989. Numerical Recipes. The Art of Scientific Computing, Cambridge University Press, Cambridge, U.K. 523–528.

Rex, S., and G. Schwarz. 1998. Quantitative studies on the melittin-induced leakage mechanism of lipid vesicles. *Biochemistry.* 37: 2336–2345.

Ross, S. M. 1989. Introduction to Probability Models, 4 Ed. Academic Press, San Diego, CA. 486–488.

Schwarz, G., and G. Beschiaschvili. 1989. Thermodynamic and kinetic studies on the association of melittin with a phospholipid bilayer. *Biochim. Biophys. Acta.* 979:82–90.

Schwarz, G., R. T. Zong, and T. Popescu. 1992. Kinetics of melittin induced pore formation in the membrane of lipid vesicles. *Biochim. Biophys. Acta.* 1110:97–104.

Selsted, M. E., M. J. Novotny, W. L. Morris, Y.-Q. Tang, W. Smith, and J. S. Cullor. 1992. Indolicidin, a novel bactericidal tridecapeptide amide from neutrophils. *J. Biol. Chem.* 267:4292–4295.

Sessa, G., J. H. Freer, G. Colacicco, and G. Weismann. 1969. Interaction of a lytic polypeptide, melittin, with lipid membrane systems. *J. Biol. Chem.* 244:3575–3582.

Skehel, J. J., and D. C. Wiley. 1998. Coiled coils in both intracellular vesicle and viral membrane fusion. *Cell.* 95:871–874.

Smith, R., F. Separovic, T. J. Milne, A. Whittaker, F. M. Bennett, B. A. Cornell, and A. Makriyannis. 1994. Structure and orientation of the pore-forming peptide, melittin, in lipid bilayers. *J. Mol. Biol.* 241: 456–466.

Strom, R., F. Podo, C. Crifo, C. Berthet, M. Zulauf, and G. Zaccai. 1983. Structural aspects of the interaction of bee venom peptide melittin with phospholipids. *Biopolymers.* 22:391–396.

Takei, J., A. Remenyi, and C. E. Dempsey. 1999. Generalised bilayer perturbation from peptide helix dimerisation at membrane surfaces: vesicle lysis induced by disulphide-dimerised melittin analogues. *FEBS Lett.* 442:11–14.

Terwilliger, T. C., and D. Eisenberg. 1982a. The structure of melittin. I. Structure determination and partial refinement. *J. Biol. Chem.* 257: 6010–6015.

Terwilliger, T. C., and D. Eisenberg. 1982b. The structure of melittin. II. Interpretation of the structure. *J. Biol. Chem.* 257:6016–6022.

Terwilliger, T. C., L. Weisman, and D. Eisenberg. 1982. The structure of melittin in the form I crystals and its implication for melittin's lytic and surface activities. *Biophys. J.* 37:353–361.

Vogel, H., and F. Jähnig. 1986. The structure of melittin in membranes. *Biophys. J.* 50:573–582.

Warren, B. E. 1969. X-ray Diffraction, Addison-Wesley, Reading, MA. 35–38.

White, S. H., and M. C. Wiener. 1995. Determination of the structure of fluid lipid bilayer membranes. *In* Permeability and Stability of Lipid Bilayers, E. A. Disalvo and S. A. Simon, editors. CRC Press, Boca Raton.1–19.

White, S. H., and M. C. Wiener. 1996. The liquid-crystallographic structure of fluid lipid bilayer membranes. *In* Membrane Structure and Dynamics, K. M. Merz and B. Roux, editors. Birkhäuser, Boston.127–144.

White, S. H., W. C. Wimley, A. S. Ladokhin, and K. Hristova. 1998. Protein folding in membranes: determining the energetics of peptide–bilayer interactions. *Methods Enzymol.* 295:62–87.

Wiener, M. C., and S. H. White. 1991a. Fluid bilayer structure determination by the combined use of X-ray and neutron diffraction. I. Fluid bilayer models and the limits of resolution. *Biophys. J.* 59:162–173.

Wiener, M. C., and S. H. White. 1991b. Fluid bilayer structure determination by the combined use of X-ray and neutron diffraction. II. "Composition-space" refinement method. *Biophys. J.* 59:174–185.

Wiener, M. C., and S. H. White. 1991c. Transbilayer distribution of bromine in fluid bilayers containing a specifically brominated analog of dioleoylphosphatidylcholine. *Biochemistry.* 30:6997–7008.

Wiener, M. C., and S. H. White. 1992. Structure of a fluid dioleoylphosphatidylcholine bilayer determined by joint refinement of x-ray and neutron diffraction data. III. Complete structure. *Biophys. J.* 61: 434–447.

Wimley, W. C., and S. H. White. 1996. Experimentally determined hydrophobicity scale for proteins at membrane interfaces. *Nature Struct. Biol.* 3:842–848.

Woolfson, M. M. 1970. X-ray Crystallography, Cambridge University Press, Cambridge. U.K. 30–45.

Wu, Y., H. W. Huang, and G. A. Olah. 1990. Method of oriented circular dichroism. *Biophys. J.* 57:797–806.